Desalination and Water Treatment
www.deswater.com

doi: 10.5004/dwt.2019.22922

137 (2019) 334–344
January

Removal of methylene blue from water solution by modified nanogoethite by Cu

Farhad Salimi[a,*], Hesam Rahimi[a], Changiz Karami[b]

[a]*Department of Chemical Engineering, Kermanshah Branch, Islamic Azad University, Kermanshah, Iran, emails: f.salimi@iauksh.ac.ir (F. Salimi), hesam_rahimi14@yahoo.com (H. Rahimi)*
[b]*Nanodrug Delivery Research Center, Kermanshah University of Medical Sciences, Kermanshah, Iran, email: changiz.karami@gmail.com*

Received 10 November 2017; Accepted 08 August 2018

ABSTRACT

In this study, nanocopper goethite (Cu-goethite) was synthesized and used to adsorb of methylene blue (MB) solution. The prepared nanoparticles were characterized by scanning electronic microscopy (SEM), energy dispersed X-ray spectroscopy (EDS), mapping image, X-ray diffraction (XRD), Fourier-transform infrared spectroscopy (FTIR) and the N_2 absorption (BET specific surface area) and pore size distribution analysis. The effects of experimental parameters, that is, pH, contact time, temperature, and initial concentration, were studied on adsorption. The results indicated that the optimum conditions for 40 mg L^{-1} MB solution were pH = 9 and 5 g L^{-1} Cu-goethite as well as pH of 10 and 7 g L^{-1} goethite along with the contact time of 30 min. Besides, the equilibrium sorption data were fitted into Langmuir, Freundlich, Temkin, and Dubinin–Radushkevich isotherms. The results also revealed that the equilibrium data were perfectly represented by the Langmuir isotherm for the adsorbents. The pseudo-first-order and pseudo-second-order models were employed to analyze the kinetics data and the adsorption behavior was better described by the pseudo-second-order model. Moreover, thermodynamic parameters have been evaluated and it has been found that the sorption process was spontaneous and exothermic in nature. Cu-goethite as an alternative adsorbent can be used for dye removal in wastewater treatment processes in the future environment governance.

Keywords: Cu-goethite; Adsorption; Methylene blue; Isotherm

1. Introduction

Synthetic dyes, as among the most hazardous materials in industrial effluents, are chemical compounds widely used by textile, food, pharmaceutical and cosmetic industries for dyeing materials, fabrics and tracer compounds [1]. There are over 10,000 kinds of commercial dyes and over 70,000 tons of dyes are produced annually [2]. The characteristics and uses of synthetic dyes are well reviewed with dyes belonging to the azo group being the most widely used by textile industries [3]. As is known, acidic, basic, reactive, disperse, and direct dyes, which usually have an aromatic structure and azo groups are common dyes. Moreover, these dyes in wastewater decrease the transparency of water, consume oxygen, and elevate biochemical oxygen demand, and thus destroy aquatic life [4,5]. Therefore, from both environmental and health perspectives, dye detoxification prior to the discharge of wastewater from dye industries is crucial. As a result, the removal of dyes from industrial effluents has attracted growing attention in the past decades. To this end, physical and chemical techniques such as chemical oxidation, membrane separation, coagulation/flocculation, and ion exchange can be carried out for wastewater treatment [6–8]. Unfortunately, most of these techniques are expensive, requiring a large amount of materials, and not environmentally friendly. Biological treatment, which involves exploiting living and nonliving biomass for dye decolorization is a cost-effective and environmentally friendly alternative [9–11]; a wide range of materials including zeolite, clay, activated carbon, polymer, eggshell particles, etc., have been reported to adsorb dyes [12–20]. Nonetheless, there are disadvantages associated with

* Corresponding author.

these materials such as low dye removal efficiency [21] and dye transfer from liquid phase to solid phase. Thus, development of new materials with good adsorption capacity, large surface area, and small diffusion resistance is still crucial. Synthetic goethite is one of the most important phases of iron oxides because of its application as an adsorbent for various toxic cations and anions due to chemical reactions occurring at specific surface sites. Incorporation of foreign di-, tri-, and tetra-valent metal species as Al, Cr, Cd, Co, Cu, Ni, Pb, V, Mn, and Zn into the structures of goethite through isomorphous substitution can modify their properties such as crystal size, morphology, stability, and dissolution behavior.

In addition, copper ions are added to the nanogoethite structure during synthesis, leading to their increased surface area and further use as an adsorbent to remove organic contaminants. The main objective of the present study was to evaluate the feasibility of applying Cu-goethite to the MB removal from aqueous solutions. We focused on enhancing adsorption capacity and reducing adsorption cost of toxic MB. To this end, first, Cu ions were loaded in the synthesized nanogoethite. Then, Cu-goethite was synthesized and characterized with scanning electronic microscopy (SEM), Fourier-transform infrared spectroscopy (FTIR), X-ray powder diffraction (XRD), and transmission electron microscopy (TEM) analysis. The effects of experimental parameters including pH, contact time, temperature, and initial concentration were studied on adsorption and the studies of kinetic, equilibrium adsorption, and thermodynamic were performed. At the end, Cu-goethite was compared with goethite.

2. Materials and methods

2.1. Materials

Iron nitrate (Fe $(NO_3)_3.9H_2O$ with a purity of 99%), potassium hydroxide (KOH with a purity of 99.99%), copper (II) sulfate ($CuSO_4{\cdot}5H_2O$ with a purity of 99%), sodium hydroxide (NaOH with a purity of 99.99%), and other chemicals and reagents used were of analytical grade such as methylene blue (MB), hydrochloric acid, nitric acid, and double distilled water.

2.2. Preparation method of nanogoethite and modified nanogoethite with Cu

Pure goethite nanorods were synthesized following the same procedure as mentioned in an early study [22]. Briefly, 10 M NaOH was added dropwise to Fe $(NO_3)_3.9H_2O$ solution until attainment of a pH of 12. A homogeneous dark brownish suspension was formed at this pH. The resulting suspension was placed into polyethylene bottles and aged at 60°C for 24 h. The aged suspensions were filtered and washed with water until the filtrates were free of nitrate, and the samples were dried at 60°C in an air oven for 24 h. The Cu doped goethite nanoparticles were prepared by using in situ Cu solution during the precipitation process. Briefly, 10 M NaOH was added dropwise at a burette to a continuously stirred prehomogeneous solution containing required amounts of $CuSO_4{\cdot}5H_2O$ and Fe $(NO_3)_3.9H_2O$ until attainment of a pH of 12. A homogeneous dark brownish suspension was formed at this pH. The resulting suspension was placed into polyethylene bottles and aged at 60°C for 24 h. The aged suspensions were filtered and washed with water until the filtrates were free of nitrate and sulfate, and the samples were dried at 60°C in an air oven for 24 h [22].

2.3. Instruments

UV–vis absorption spectra were acquired on a Cary 100 UV–vis spectrometer (Varian, USA) at room temperature (23°C–25°C) and using a double beam. FT-IR spectra were measured on a PerkinElmer pressed into KBr pellets and is reported in wave numbers (cm^{-1}). And field emission scanning electron microscopy images were obtained using a HITACHI S-4160 field emission SEM. XRD analysis on a Philips PANalytical X'Pert PRO diffractometer with CuKα radiation. Typically, a scanning velocity of 1.5°min^{-1} was used to scan the peaks of the adsorbent diffraction pattern in the 2θ range between 5° and 80°. A Metrohm 692 pH meter (Herisau, Switzerland) was used for pH measurements.

2.4. Method

In this study, different experiments were performed in order to investigate the adsorption of MB using the modified nano-Cu-goethite and goethite. To evaluate the adsorption of the MB dye, several different tests were performed. All the batch adsorption experiments were carried out as desired, that is, 0.001–0.2 g; adsorbents powder was mixed with 10 mL MB dye solution and appropriate pH after shaking in a constant temperature oscillator at a speed of 200 rpm. The pH of the dye solution was adjusted to different pH values between 1 and 13 using HCl (0.1 mol L^{-1}) or NaOH (0.1 mol L^{-1}) solution. The resulting solution was poured into a test tube and then placed in a centrifuge at a 4,000 rpm speed for 10 min so that the nanoadsorbent would remain at the bottom of the test tube. Ultimately, the amount of adsorption of the resulting solution was calculated using UV/vis. Percentage of adsorption was calculated using the following equation:

$$\%\text{Removal} = \frac{\left(C_i - C_f\right)}{C_i} \times 100 \tag{1}$$

where C_i and C_f are the initial and final concentrations of MB in the solution, respectively. The MB with a purity of 99% used for preparing the solution has been bought from Merck Company in Germany. Various concentrations of MB have been used to prepare the 5–120 mg L^{-1} solution and the various amount of adsorption was reviewed with goethite and Cu-goethite. Then, the following equation was used to determine the adsorption capacity:

$$q_e = \frac{\left(C_0 - C_e\right)V}{M} \tag{2}$$

where C_0 (mg L^{-1}) and C_e (mg L^{-1}) are the initial and equilibrium concentrations of dye, respectively. The V (L) and m (g) are the solution volume and the mass of the adsorbent, respectively [23,24].

2.5. Sorption isotherms

Adsorption isotherm describes how the adsorbent interacts with the substance been adsorbed and they can provide

important information about the nature of the interaction between adsorbate and adsorbent and also it can be used to determine the adsorption capacity of adsorbent. In this work, the isotherms data were fitted by the following models: Langmuir, Freundlich, Temkin, and Dubinin–Raduskevich.

Langmuir considered adsorption as an ideal adsorption on an ideal surface. This model assumes that adsorption can only be done in constant sites and it can only maintain one adsorbing molecule at a time (single-layered). In addition, when molecules are adsorbed on the surface of the adsorbent, they cannot be separated [25]. Their adsorption equation is as follow:

$$\frac{c_e}{q_e} = \frac{c_e}{q_{\max}} + \frac{1}{b \times q_{\max}} \tag{3}$$

where $q_{\max}$ (mg g^{-1}) is the monolayer adsorption capacity, b (L g^{-1}) is the Langmuir constant that is related to the free energy of adsorption, while C_e (mg L^{-1}) is the equilibrium concentration of adsorbate in solution and q_e (mg g^{-1}) is the concentration of adsorbate on the surface of adsorber. The essential characteristics of Langmuir isotherm can be explained using a dimensionless constant, R_L, known as separation factor, which is calculated using the following equation:

$$R_L = \frac{1}{\left(1 + bC_0\right)} \tag{4}$$

where C_0 (mg L^{-1}) is the initial liquid phase concentration of analyte and b is the Langmuir adsorption constant (L mg^{-1}). The R_L value describes adsorption process to be unfavorable ($R_L > 1$), linear ($R_L = 1$), favorable ($0 < R_L < 1$), or irreversible ($R_L = 0$) [26].

Freundlich isotherm is a multisite adsorption isotherm for heterogeneity surfaces [27] and its total form has been shown in the following equation:

$$q_e = K_f C_e^{b_f} \tag{5}$$

where q_e and C_e are the parameters in Eq. (5) and the numerical value of K_f presents adsorption capacity and shows energetic heterogeneity of adsorption sites. The value of b_f between 0 and 1 indicates favorable adsorption process. If the value of $b_f \geq 2$, this indicates that the adsorption processed is difficult to carry out.

Temkin isotherm is one of the earliest reported isotherm, which assumes linear decrease of the adsorption heat with increasing coverage [28]. As implied in the equation, its derivation is characterized by a uniform distribution of binding energies (up to some maximum binding energy) was carried out by plotting q_e against ln C_e and the constants were determined from the slope and intercept. The model is given by the following equations [28]:

$$q_e = \frac{RT}{b} \ln\left(A_T C_e\right) \tag{6}$$

$$q_e = \frac{RT}{b} \ln\left(A_T\right) + \frac{RT}{b} \ln\left(C_e\right) \tag{7}$$

$$B = \frac{RT}{b} \tag{8}$$

$$q_e = B \ln\left(A_T\right) + B \ln\left(C_e\right) \tag{9}$$

where A_T, b_T, R, T, and B are A_T = Temkin isotherm equilibrium binding constant (L g^{-1}); R = universal gas constant (8.314 J mol^{-1} K^{-1}); b_T = Temkin isotherm constant; and T = temperature at 298 K and B = constant related to heat of sorption (J mol^{-1}).

Dubinin–Radushkevich isotherm is generally applied to express the adsorption mechanism with a Gaussian energy distribution onto a heterogeneous [24,29]. The model has often successfully fitted high solute activities and the intermediate range of concentrations data well. This model is as follows:

$$q_e = \left(q_s\right) \exp\left(-K_{\text{ad}} \varepsilon^2\right) \tag{10}$$

$$\ln q_e = \ln\left(q_s\right) - \left(K_{\text{ad}} \varepsilon^2\right) \tag{11}$$

where q_e, q_s, K_{ad} are q_e = amount of adsorbate in the adsorbent at equilibrium (mg g^{-1}); q_s = theoretical isotherm saturation capacity (mg g^{-1}); K_{ad} = Dubinin–Radushkevich isotherm constant (mol^2 kJ^{-2}), and = Dubinin–Radushkevich isotherm constant. The parameter ε can be calculated as:

$$\varepsilon = RT \ln\left(1 + \frac{1}{C_e}\right) \tag{12}$$

where R, T, and C_e represent the gas constant (8.314 J mol^{-1} K), absolute temperature (K), and adsorbate equilibrium concentration (mg L^{-1}), respectively.

2.6. Kinetics studies

To match the experimental data on adsorbent, different kinetics models have been reported including pseudo-first and pseudo-second-order kinetics equations. One of the most important factors to determine the optimal contact time is speed prediction and adsorption process that is controlled by kinetics. In this study, the kinetics of adsorption of MB by modified and unmodified goethite adsorbent was investigated using pseudo-first and pseudo-second-order kinetics equations. The linear form of pseudo-first and pseudo-second-order kinetics equations are respectively shown in Eqs. (13) and (14) [30,31].

$$\ln\left(q_{e-}q_t\right) = \text{Ln}\left(q_e\right) - k_1 \times t \tag{13}$$

$$\frac{t}{q_t} = \frac{1}{k_2 \left(q_e\right)^2} + \frac{t}{q_e} \tag{14}$$

q_e (mg g^{-1}) and q_t (mg g^{-1}) are the amount adsorption capacities at the equilibrium and time t (min), respectively. The k_1 and k_2 are the first and second-rate constant (L min^{-1}), respectively.

2.7. Regeneration study of adsorbent

In the desorption experiments, ethanol (20% v/v) was used as the desorbing agent. 2 mL of the above desorbing agent was mixed with the adsorbent loaded MB sample and shaken for 60 min at 298 K. Then, the samples were separated from the solution by magnetic separation and washed with ultrapure water three times. The residual adsorbent was subjected again to the adsorption process [32].

3. Results and discussions

In this study, Cu-goethite and goethite particles were synthesized by mixing $CuSO_4{\cdot}5H_2O$ and Fe $(NO_3)_3{\cdot}9H_2O$ until attainment of a pH of 12. Furthermore, the Cu-goethite and goethite were characterized using XRD, SEM, EDX, mapping, and FT-IR spectra.

3.1. The XRD pattern

According to the XRD patterns of Cu-goethite and goethite particles shown in Fig. 1, which demonstrates the reflections characteristic of goethite is PDF No. 29–0713 and the reflections characteristic of Cu-goethite is JCPDS card 85-1326. In addition to, in the XRD patterns, the result showed the peaks at 43.3°, 50.4°, and 72.3 in Fig. 1(b) add to Fig. 1(a) that it was proven the structure of Cu-goethite. The diameter of Cu-goethite and goethite can be achieved by the Scherrer equation as follows

$$D = \frac{k \times \lambda}{\beta \times \cos\theta} \tag{15}$$

where D is the mean size of the ordered (crystalline) domains; K is a dimensionless shape factor, with a value close to unity. The shape factor has a typical value of about 0.9, but varies with the actual shape of the crystallite; λ is the X-ray; Wavelength; β is the line broadening at half the maximum intensity (FWHM), after subtracting the instrumental line broadening, in radians. This quantity is also sometimes denoted as $\Delta(2\theta)$; θ is the Bragg angle. According to the half-height of peak list of goethite and Cu-goethite, the crystallite diameters of them were calculated using the Scherrer equation [Eq. (15)]. Therefore the estimated crystallite diameters of goethite nanorods in $2\theta = 35.79°$ were around 11.08 nm and for Cu-goethite in $2\theta = 21.31°$ is 17.29 nm.

3.2. The FTIR spectrum

The nano-Cu-goethite and goethite adsorbents were measured by FTIR and the obtained spectrums are presented in Fig. 2. The FTIR spectrum controls the presence of many functional groups. Fig. 2 for goethite is characteristic of α-FeOOH. The sharp, distinct, and intense pair of bands at around 891 and 794 cm^{-1} can be assigned to the Fe–O–H bending vibration; consequently, the bands at 622 and 476 cm^{-1} can be assigned to the Fe–O stretching vibration [33].

Fig. 2 shows a strong bond in 3,412.75 cm^{-1} attributed to the stretching vibration of surface H_2O molecules or the hydrogen bonded surface OH groups [34]. The bond is at 2,926.17 cm^{-1} related to the C–H vibrations; whereas the sharp and intense band at 1,617.87 cm^{-1} is typical for the bending vibration of –OH or N=C group. Strong band at 1,361 cm^{-1} can be assigned to the presence of CO_3^{-2} due to the contamination by atmospheric CO_2 [35].

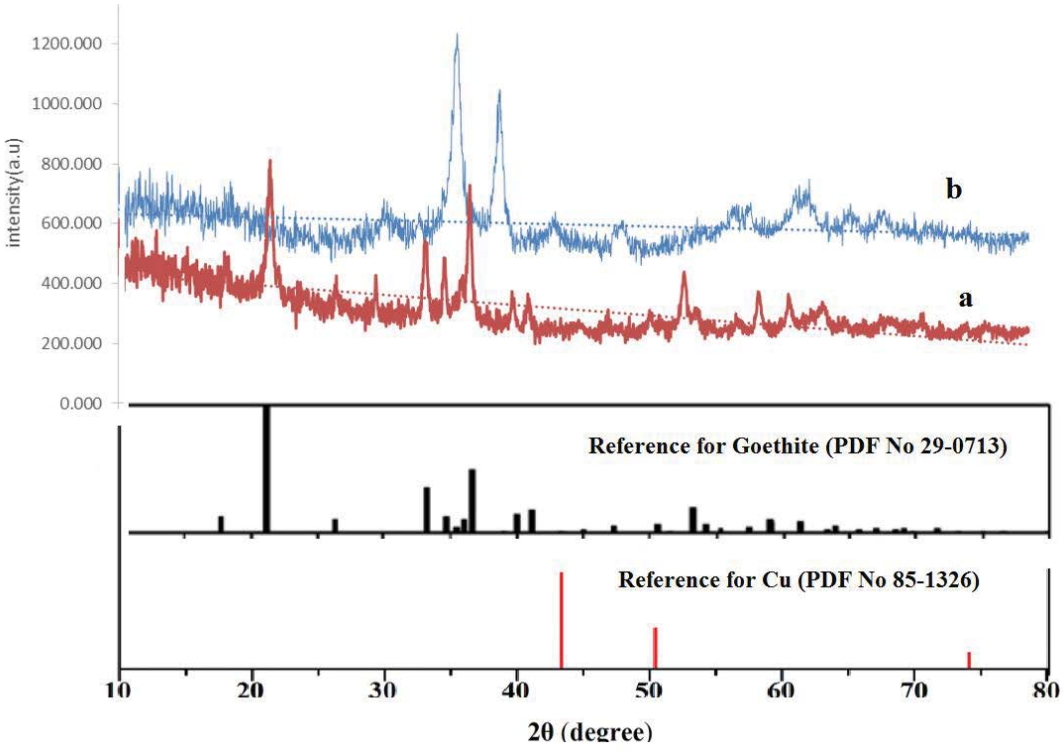

Fig. 1. XRD pattern of the nanogoethite (a) and Cu-goethite (b).

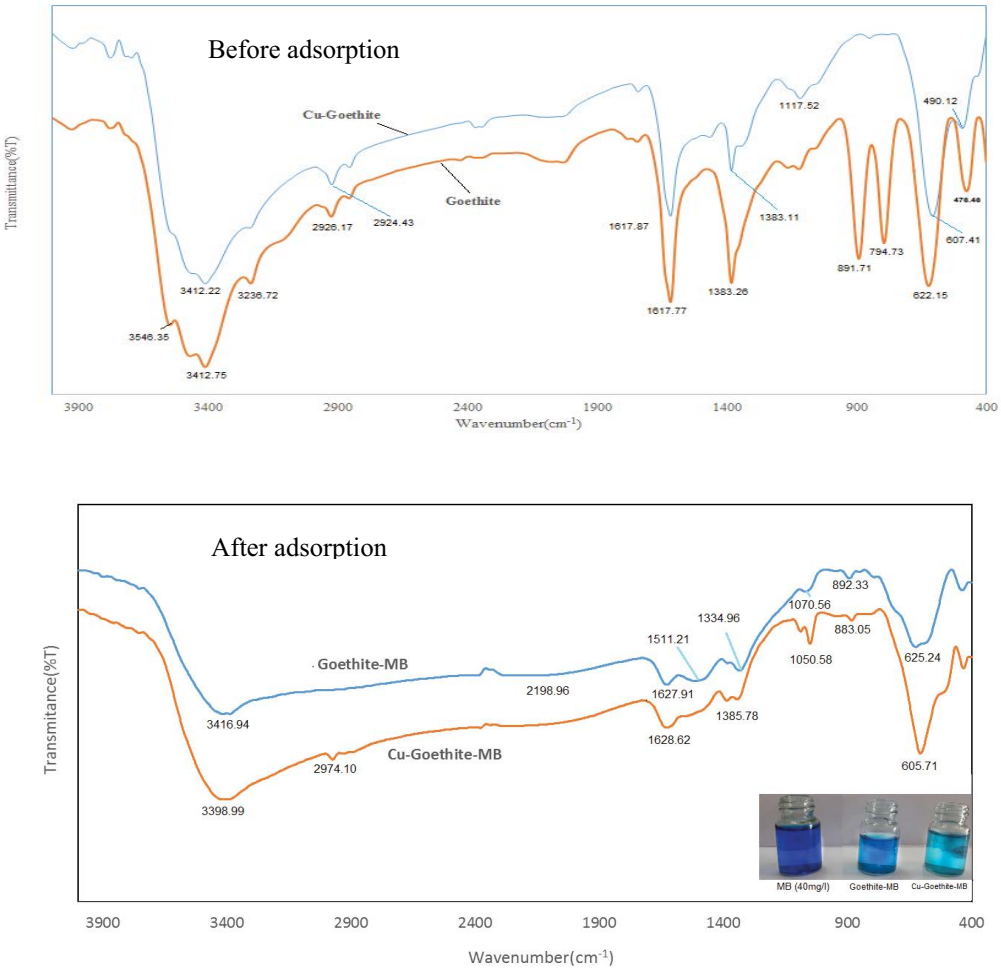

Fig. 2. the FTIR spectrum of the goethite and Cu-goethite before and after adsorption.

The spectrum of nano-Cu-goethite (Fig. 2) is similar to goethite spectrum with this difference that the peaks of 794 and 891.7 cm^{-1}, related to the Fe–O–H bending vibration, have been removed. Besides, the high-frequency mode at 607.41 cm^{-1} may be attributed to the Cu_2O stretching [36].

To obtain evidence for the adsorption of MB into adsorbents, the FTIR spectra of MB loaded adsorbents are shown in Fig. 2. Results indicate that the band near 1,385 cm^{-1} is related to the $–CH_3$ peak and the peaks at 1,397–1,323 cm^{-1} region and the feature conforming to the C=C skeleton stretching at 1,628 cm^{-1} creates from the aromatic ring vibrations of MB [37].

3.3. The SEM, EDS, mapping, and the BET analysis

SEM observation of the micrographs of the goethite and Cu-goethite samples given in Fig. 3 shows distinct changes in the size and geometrical shape of the Cu-substituted a-FeOOH particles. The undoped goethite showed elongated particles which were acicular or rod type and the diameter of the nanoparticles was about 150 nm (Fig. 3(a)). The shaped doping Cu-goethite was a round and the diameter of the nanoparticles was about 100 nm. However, it was shown that the Cu-goethite particles had much smaller widths and lengths (Fig. 3(b)). This may be a consequence of nonuniform distribution of Cu-dopant. In order to detect elements present in the samples, EDX and mapping analysis were carried out.

The spectrum EDX indicates the presence of copper, oxygen, and iron. The presence of Na was from the substrate. The formation of Cu was confirmed from the EDX. The spectrum mapping indicated the presence of copper, oxygen, and iron in the nano-Cu-goethite (Fig. 4).

In Fig. 4, the adsorption and desorption isotherms, the pore size distribution for the goethite/Cu-goethite is illustrated. The type IV isotherm characteristic with an adsorption hysteresis indicated that the nanoporous structure exists on the adsorbents [38]. The specific surface area and pore size of the goethite and Cu-goethite were 5.63 $m^2\ g^{-1}$, 94.11 $m^2\ g^{-1}$, and 1–5.5, 1–58 nm, respectively, and then respective average pore size was evaluated to be 5.7114 and 7.2307 nm. The pore volumes of goethite and Cu-goethite were 0.0080445 and 0.1701 $cm^3\ g^{-1}$, respectively. The conclusion is consistent with the SEM.

3.4. The effect of pH

The pH is an important factor affecting the removal of dyes and metal ions from aqueous solutions. In low pH, the adsorbent has positive charge because a pH lower than

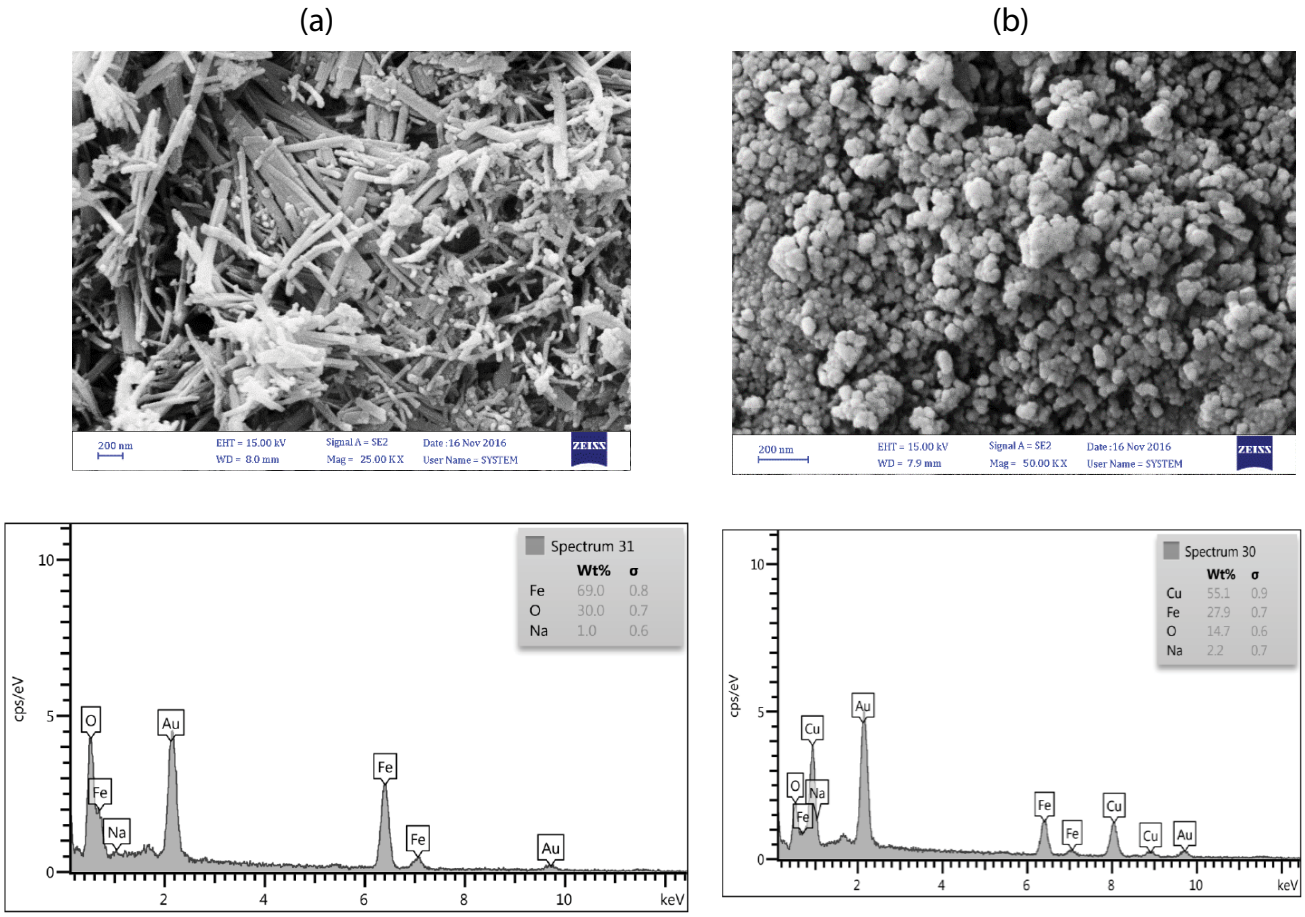

Fig. 3. SEM micrograph for the goethite (a) and Cu-goethite (b).

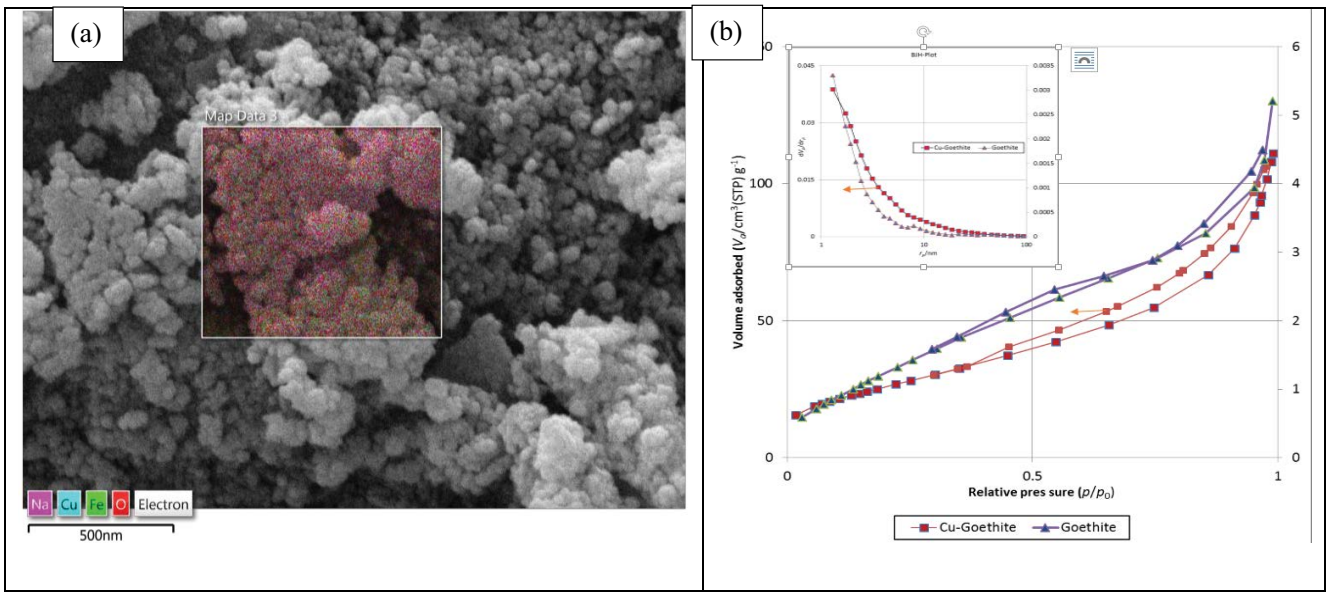

Fig. 4. (a) Mapping image for the Cu-goethite, (b) N2 absorption isotherms of adsorbents.

isoelectric or point of zero charge (PZC); in other words, ($pH < pH_{PZC}$). At strong acidic pHs (Fig. 5), high amounts of protons present in the solution competed with MB for occupying the active sites of the sorbent and decreased the complexation of MB with the adsorbent. In addition, repulsive force between MB cations and positive charge of the sorbent, at pHs < pH_{PZC}, prevented to reach enough MB near the sorbent. Hence, strong acidic conditions are not suitable for MB removal by the proposed sorbent.

By increasing the pH these problems tend to decrease and removal extent tends to increase. In high pH ($pH \geq pH_{PZC}$), the adsorbent has negative charge which leads to high adsorption. This is caused by the fact that when the MB is in the solution, it has positive charge and is adsorbed to the surface of the adsorbent in which pH has a negative charge ($pH > pH_{PZC}$), which helps the adsorption. In order to study of pH, 0.07 g of adsorbent was added to 10 mL of dye solution of MB at a concentration of 40 mg L^{-1} and its pH was set from 2 to 11 and then they were put on the mechanical shaker for 30 min.

The pH of PZC of the goethite, PZC, was 9 [39]. The results of Fig. 5 show that the best MB removal for goethite (86.7%) and Cu-goethite (90%) was obtained at pH = 10, 9, respectively. Intuitively, MB cationic dye can be adsorbed easily on the surface of the negatively charged adsorber at alkaline pHs. Although strong adsorption of the MB took place at high pH, a high extent of this removal was due to surface adsorption of MB molecules. Furthermore, the concentration of hydroxyl radicals decreased at high pH (due to reaction of hydroxyl radicals with hydroxyl anions at high OH concentrations), which in turn decreased the adsorption rate [40,41].

3.5. The effect of adsorbent dosage

Various amounts of the goethite and nano-Cu-goethite were filled in separate columns. Model solutions 10 mL, with a concentration of 40 mg L^{-1} and the adjusted pH with the optimal rate of each metal (pH = 9, 10 for goethite and nano-Cu-goethite, respectively) was added to each column. Fig. 6 shows the results of the effect of mass of the adsorbent on the adsorption.

As is clear from the results, increase of the adsorbent amount from 0.001 to 0.2 g was accompanied with the increase of the color removal percentage. The obtained optimal mass for the studied adsorbent equaled 0.01 g. In general,

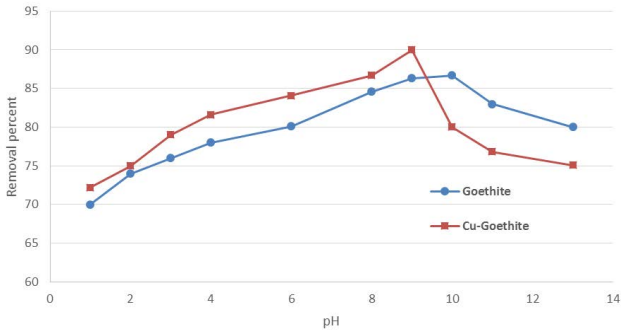

Fig. 5. Effect of pH on adsorption of dye MB on the adsorbents (conditions: 7 mg adsorbent, 10 mL of 40 mg L^{-1} of cationic dye).

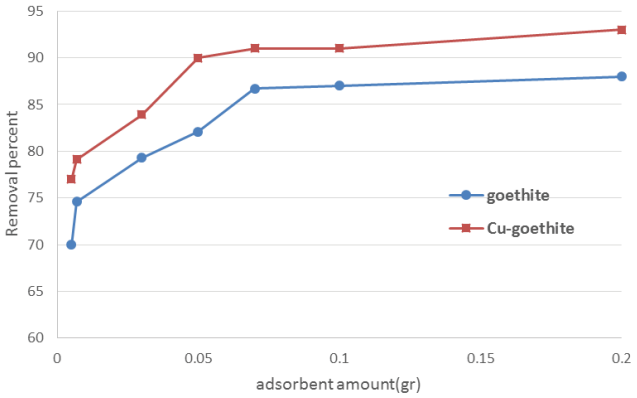

Fig. 6. Effect of adsorbent amount on cationic dye MB adsorption on adsorbents (conditions: 10 mL of 40 mg L^{-1} of dyes, pH = 9, 10 for goethite and Cu-goethite, respectively).

color adsorption capacity in the adsorbent increased with the increase of the adsorbent mass. This is because increase of the adsorbent mass was accompanied with the increase of the special surface and adsorption sites [42,43,25].

The results indicated that the adsorption rate of the proposed mixture was first increased and then decreased with the increase in the adsorption quantity to 0.07 g for goethite (0.05 g for Cu-goethite). The increase of the MB removal efficiency was because of increasing the available surface area or the active sites of the catalyst. At a higher level of adsorbent dosage, the adsorption rate reduce, although the reactive sites were increased. This is due to the fact that concentration is the driving force of the MB dye for occupation of the available adsorption sites. When most of the MB dyes are adsorbed, the graph becomes horizontal because the MB ions in the solutions have been finished [40]. The obtained result is in good accordance with SEM and XRD results that modification of goethite by Cu lead to a higher surface area and adsorption rate.

3.6. The effect of adsorption time

The profile of adsorption time was studied by doing batch sorption experiments so that the dependency of

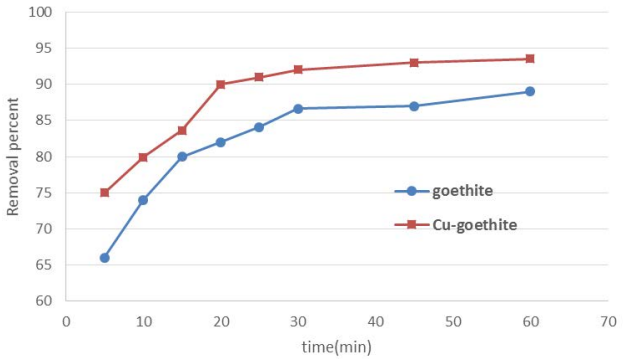

Fig. 7. Effect of contact time of cationic dye MB adsorption on adsorbents (conditions: 10 mL of 40 mg L^{-1} of dyes, pH = 9, 10 and 7, 5 g L^{-1} for goethite and Cu-goethite, respectively).

the adsorption on the time for the nano-Cu-goethite and goethite adsorbent would be specified. This test was performed over the 5–60-min interval with the change range of 5 min and the optimal time was accordingly obtained. Results of Fig. 7 show that by increasing the contact time, the removal efficiency increased and reached its optimal time at 20 min for nano-Cu-goethite and 30 min for goethite, and the removal percentage reached 90 and 86.62, respectively. The abundance and availability of empty sites on the surface of the adsorbent caused the very quick adsorption of MB from the aqueous solution onto the adsorbent in the first few minutes [44,45].

3.7. The effect temperature

In Fig. 8 (right), the effect of temperature on the MB adsorption is shown. The results show that adsorption of MB had the highest dye removal by Cu-goethite (goethite) with pH = 9 (pH = 10), an adsorption rate of 0.05 (0.07 g), and 40 mg L^{-1} concentration of MB at 30 min time of 25°C, while dye removal decreases as temperature increases. The reason could be increased mobility of MB molecules and their adsorption decreased by surface [46].

3.8. The effect of MB dye

In order to review the adsorption capacity for the nano-Cu-goethite and goethite adsorbents, 10 mL of the model solution with concentrations in the range of 5–120 mg L^{-1} were transferred to beaker and 0.05 g (0.07 g) of the nano-Cu-goethite (goethite) adsorbent at pH = 9 (pH = 10) and then they were put on the mechanical shaker for 30 min. As shown in Fig. 8 (left), the removal rate reduces with increasing concentration of MB [47]. At low concentrations, MB is adsorbed on the vacant cites of adsorbent surface and these places are saturated and filled by increasing the concentration. When the initial concentration of MB dye is low, the number of sites available for dye adsorption on the surface of the adsorbent is very high. However, as long as the initial concentration of MB dye is increased, the number of moles of MB dye is high than the number of vacant sites. Therefore, the available sites are quickly saturated and dye removal rate decreases [23]. Results show that the maximum adsorptions are 12.24 mg g^{-1}, 7.71 mg g^{-1} for Cu-goethite and goethite.

3.9. Results of sorption isotherms and kinetics studies

In this paper, investigation of the equilibrium sorption was carried out at ambient temperature. Other physicochemical parameters were determined and four adsorption isotherm models were studied. The correlation coefficient R^2 was higher than 0.99 for Freundlich model while it was just lower than 0.94 for other models. This result suggested that the Freundlich model described the present adsorption system sufficiently well whereas the other models did not match the data satisfactorily. The Freundlich isotherm was all better than the other isotherms, implying that the adsorption process involved multimolecular layers of coverage, and heterogeneous nature of adsorptive sites on the surface of adsorbents.

As shown in Table 1, the Langmuir and Freundlich model well fitted the adsorption isotherm of the two adsorbents and the maximum adsorption capacity was calculated theoretically. The obtained value was similar to the experimental data value. The adsorption of the two adsorbents was difficult to be carried out inferring from the value of b_f obtained from the Freundlich model [48].

The information presented in Table 2 depicts how the contact time affects the adsorption process at different times. It must be noted that all the tests and experiments have been performed at ambient temperature. The results of adsorption behavior showed that the pseudo-second-order kinetic model fitted well with all experimental data (goethite: R^2 = 0.9998, Cu-goethite: R^2 = 0.9997), meaning that the adsorption rate was mainly determined by the chemical adsorption process. This fitting result indicated that the electron transfer, exchange, or sharing was generated and chemical bond was formed in the adsorption process [49]. The k_1 and k_2 are presented in Table 2.

3.10. Adsorption mechanism

The pore size and pore volume are important properties considered in the manufacture of materials as adsorbents for specific applications. The pore size and pore volume are accessible to a molecule of a given size. The physical adsorption mechanism in small pore size is mainly pore filling because the overlapping of pore; thus, larger molecules cannot access the small pore size of adsorbent. Table 1 shows

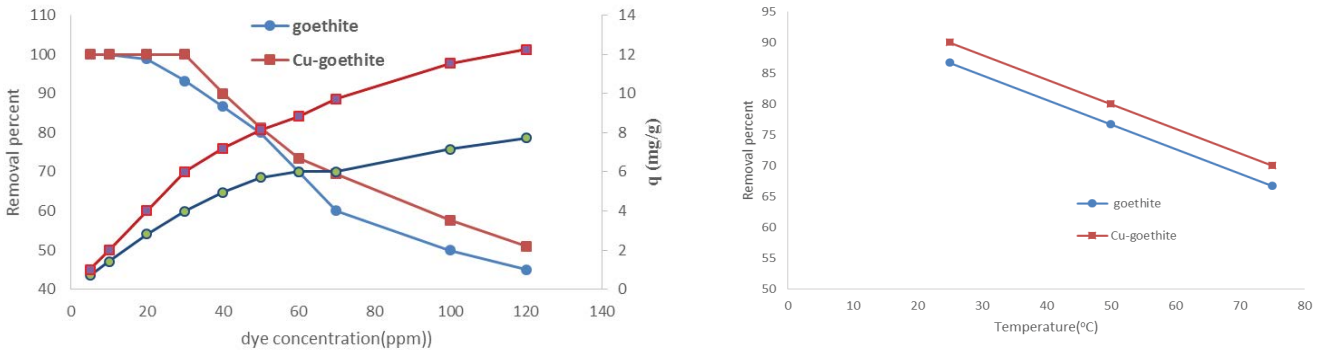

Fig. 8. Effect of initial dye concentration (left) and temperature (right) on adsorption of MB dyes (conditions: 10 mL of dyes, pH = 9, 10 and 7, 5 g L^{-1} goethite for Cu-goethite adsorbent, respectively).

Table 1
Langmuir, Freundlich, Temkin, and Dubinin–Radushkevich isotherm constants for the adsorption of MB

Adsorbent	Langmuir isotherm				Freundlich isotherm			
	Q_{max} (mg g^{-1})	$b = k_L$ (L mg^{-1})	R_L	R^2	$b_f = 1/n$	n	k_f(mg g^{-1})	R^2
Cu-goethite	12.69	0.069	0.266	0.998	2.63	0.38	0.133	0.939
Goethite	7.12	0.072	0.258	0.993	2.83	0.353	0.036	0.936
	Temkin isotherm				Dubinin–Radushkevich isotherm			
	A_T (L mg^{-1})	b_T	B	R^2	q_s (mg g^{-1})	K_{ad} (mol^2 kJ^{-1})	–	R^2
Cu-goethite	7.81	77.98	31.77	0.639	54.60	2×10^{-7}	–	0.85
Goethite	5.20	48.82	50.75	0.796	26,903	1×10^{-6}	–	0.705

the maximum adsorption capacities of the Cu-goethite more than goethite. In other words, the reason that Cu-goethite adsorbs much more MB than the goethite is most possibly related to the fact that it has the highest pore size or the pore volume (Fig. 4) [50–52].

3.11. Thermodynamic studies

The Gibb's free energy (ΔG^0), entropy (ΔS^0), and enthalpy (ΔH^0) changes for the adsorption were determined by:

$$\ln K_l = \frac{\Delta S^0}{R} - \frac{\Delta H^0}{RT} \tag{16}$$

$$\Delta G^0 = \Delta H^0 - T\Delta S^0 \tag{17}$$

where T is the solution temperature (K), R is the universal gas constant (8.314 J K^{-1} mol^{-1}) and K_l is the equilibrium constant [55]. The calculated thermodynamic parameters are demonstrated in Table 3.

Table 2
Lagergren pseudo-first-order kinetic and pseudo-second-order kinetic data

Adsorbent	Order	Pseudo-second order	Pseudo-first order
Cu-goethite	R^2	0.9997	0.9643
	k	0.0758 g mg^{-1} min^{-1}	0.0238 min^{-1}
Goethite	R^2	0.9998	0.8241
	k	0.0834 g mg^{-1} min^{-1}	0.0081 min^{-1}

The values of Gibbs free energy ΔG^0 had been calculated by knowing the ΔH^0 and the ΔS^0 and ΔH^0 were obtained from a plot of ln K_l versus $1/T$, from Eq. (16). Once these two parameters were obtained, ΔG^0 is determined from Eq. (17). The positive values of ΔS^0 suggested the increased randomness at the solid/solution interface during the adsorption [53,54]. The negative values of ΔG^0 in Table 3 revealed that the MB dye adsorption by the adsorbents was the spontaneous process. Moreover, it was observed that the ΔG^0 values decreased with temperature growth from 20°C to 60°C, indicating that the process was more efficient at higher temperature. Furthermore, from the ΔG^0 values bigger than −15 kJ mol^{-1}, it could be implied that the interactions between the adsorbent sites and dye were chemical. Moreover, according to Table 3, for dye adsorption by the adsorbents, the negative value of ΔH^0 and positive value of ΔS^0 represented that the process was exothermic with increasing in randomness at the interface of solid-solution within the adsorption [55]. The higher heat of the adsorption obtained in this work indicated that chemisorption rather than the physical adsorption was prevailing [56].

3.12. Regeneration study

The experiment about the adsorption capacity of the recycled adsorbent has been investigated by four times cycles. In this part, the initial dye concentration is 40 mg L^{-1} and the dosage of adsorbents are 5 g L^{-1} Cu-goethite and 7 g L^{-1} goethite, %20 v/v ethanol was used as eluent. From Table 4 it is clear that the adsorption percentage of adsorbent for MB has a decline from 88% to 70% for Cu-goethite and 87% to 74% for goethite after four times cycles.

Table 3
Thermodynamic parameters for the adsorption of adsorbents at different temperatures

			Δ G^o (kj mol^{-1})		
			T(°C)		
	ΔS^o (kj mol^{-1})	ΔH^o (kj mol^{-1})	20	40	60
Goethite	0.1142	–46.658	–80.120	–82.404	–84.669
Cu-goethite	0.0334	–18.737	–28.521	–29.189	–29.857

Table 4
The adsorption recycles of adsorbents

Recycle times	1	2	3	4
Goethite	87	82	79.7	74
Cu-goethite	88	80	71	70

4. Conclusion

In this research, MB was adsorbed from dye solution using goethite and modified goethite by Cu (Cu-goethite). In summary, the results of adsorption study of two adsorbents on MB indicated that the adsorption of Cu-goethite is better compared with goethite for MB adsorption. The results of the adsorption process showed that the optimum conditions for maximum adsorption of 40 mg L^{-1} MB for Cu-goethite and goethite adsorbent were contact time of 30 min, pH of 9, adsorbent of 5 g L^{-1}, contact time of 30 min, pH of 10, and adsorbent of 7 g L^{-1}, respectively. The sorption data fitted into Langmuir, Freundlich, Temkin, and Dubinin–Radushkevich isotherms of which the Langmuir Adsorption model was found to have the highest regression value for the adsorbents. Kinetics adsorption experiments were performed to determine the balance time at different concentrations of MB. The results showed that, at different concentrations, with the increase of contact time, the amount of adsorbed dye per unit weight of the adsorbent increased. Data of the experiment was fitted using two pseudo-first and pseudo-second-order models and they indicated the adsorption kinetics follows the pseudo-second-order type for Cu-goethite and goethite. Also, thermodynamic parameters have been evaluated and it has been found that the adsorption process was spontaneous and exothermic in nature.

References

[1] L. Ai, C. Zhang, F. Liao, Y. Wang, M. Li, L. Meng, J. Jiang, Removal of methylene blue from aqueous solution with magnetite loaded multi-wall carbon nanotube: kinetic, isotherm and mechanism analysis, J. Hazard. Mater., 198 (2011) 282–290.

[2] O. Legrini, E. Oliveros, A. Braun, Photochemical processes for water treatment, Chem. Rev., 93 (1993) 671–698.

[3] S. Li, Removal of crystal violet from aqueous solution by sorption into semi-interpenetrated networks hydrogels constituted of poly (acrylic acid-acrylamide-methacrylate) and amylose, Bioresour. Technol., 101 (2010) 2197–2202.

[4] R. Rakhshaee, M. Panahandeh, Stabilization of a magnetic nano-adsorbent by extracted pectin to remove methylene blue from aqueous solution: a comparative studying between two kinds of cross-likened pectin, J. Hazard. Mater., 189 (2011) 158–166.

[5] B.S. Inbaraj, B. Chen, Dye adsorption characteristics of magnetite nanoparticles coated with a biopolymer poly (γ-glutamic acid), Bioresour. Technol., 102 (2011) 8868–8876.

[6] A. Srinivasan, T. Viraraghavan, Decolorization of dye wastewaters by biosorbents: a review, J. Environ. Manage., 91 (2010) 1915–1929.

[7] S.B. Younes, Z. Bouallagui, S. Sayadi, Catalytic behavior and detoxifying ability of an atypical homotrimeric laccase from the thermophilic strain Scytalidium thermophilum on selected azo and triarylmethane dyes, J. Mol. Catal. B: Enzym., 79 (2012) 41–48.

[8] T. Robinson, G. McMullan, R. Marchant, P. Nigam, Remediation of dyes in textile effluent: a critical review on current treatment technologies with a proposed alternative, Bioresour. Technol., 77 (2001) 247–255.

[9] M.T. Yagub, T.K. Sen, S. Afroze, H.M. Ang, Dye and its removal from aqueous solution by adsorption: a review, Adv. Colloid Interface Sci., 209 (2014) 172–184.

[10] C. Park, M. Lee, B. Lee, S.-W. Kim, H.A. Chase, J. Lee, S. Kim, Biodegradation and biosorption for decolorization of synthetic dyes by *Funalia trogii*, Biochem. Eng. J., 36 (2007) 59–65.

[11] M. Taha, E. Adetutu, E. Shahsavari, A. Smith, A. Ball, Azo and anthraquinone dye mixture decolourization at elevated temperature and concentration by a newly isolated thermophilic fungus, Thermomucor indicae-seudaticae, J. Environ. Chem. Eng., 2 (2014) 415–423.

[12] R. Cornell, U. Schwertmann, Dissolution, the Iron Oxides: Structure, Properties, Reactions, Occurrences and Uses, John Wiley & Sons, 2nd ed., 2003, pp. 297–344.

[13] P. Senthil Kumar, R. Sivaranjanee, U. Vinothini, M. Raghavi, K. Rajasekar, K. Ramakrishnan, Adsorption of dye onto raw and surface modified tamarind seeds: isotherms, process design, kinetics and mechanism, Desal. Wat. Treat., 52 (2014) 2620–2633.

[14] P.S. Kumar, J. Pavithra, S. Suriya, M. Ramesh, K.A. Kumar, *Sargassum wightii*, a marine alga is the source for the production of algal oil, bio-oil, and application in the dye wastewater treatment, Desal. Wat. Treat., 55 (2015) 1342–1358.

[15] V. Mathivanan, S. Geetha Manjari, R. Ineya, R. Saravanathamizhan, P. Senthil Kumar, K. Ramakrishnan, Enhanced photocatalytic decolorization of reactive red by sonocatalysis using TiO_2 catalyst: factorial design of experiments, Desalin. Wat. Treat., 57 (2016) 7120–7129.

[16] P.S. Kumar, S.J. Varjani, S. Suganya, Treatment of dye wastewater using an ultrasonic aided nanoparticle stacked activated carbon: kinetic and isotherm modelling, Bioresour. Technol., 250 (2018) 716–722.

[17] F. Salimi, M. Eskandari, C. Karami, Investigating of the methylene blue adsorption of wastewater using modified nano-zeolite by copper, Desal. Wat. Treat., 85 (2017) 206–214.

[18] F. Salimi, M. Abdollahifar, P. Jafari, M. Hidaryan, A new approach to synthesis and growth of nanocrystalline AlOOH with high pore volume, J. Serb. Chem. Soc., 82 (2017) 203–213.

[19] F. Salimi, K. Tahmasobi, C. Karami, A. Jahangiri, Preparation of modified nano-SiO_2 by bismuth and iron as a novel remover of methylene blue from water solution, J. Mex. Chem. Soc., 61 (2017) 250–259.

[20] F. Salimi, S.S. Emami, C. Karami, Removal of methylene blue from water solution by modified nano-boehmite with bismuth, Inorg. Nano-Met. Chem., 48 (2017) 31–40.

[21] M. Alvarez, E.H. Rueda, E.E. Sileo, Simultaneous incorporation of Mn and Al in the goethite structure, Geochim. Cosmochim. Acta, 71 (2007) 1009–1020.

[22] K. Rout, A. Dash, M. Mohapatra, S. Anand, Manganese doped goethite: structural, optical and adsorption properties, J. Environ. Chem. Eng., 2 (2014) 434–443.

[23] H. Han, W. Wei, Z. Jiang, J. Lu, J. Zhu, J. Xie, Removal of cationic dyes from aqueous solution by adsorption onto hydrophobic/hydrophilic silica aerogel, Colloids Surf., A., 509 (2016) 539–549.

[24] A. Günay, E. Arslankaya, I. Tosun, Lead removal from aqueous solution by natural and pretreated clinoptilolite: adsorption equilibrium and kinetics, J. Hazard. Mater., 146 (2007) 362–371.

[25] J.-Z. Guo, B. Li, L. Liu, K. Lv, Removal of methylene blue from aqueous solutions by chemically modified bamboo, Chemosphere, 111 (2014) 225–231.

[26] S.Z. Ali, M. Athar, M. Salman, M.I. Din, Simultaneous removal of Pb (II), Cd (II) and Cu (II) from aqueous solutions by adsorption on *Triticum aestivum*-a green approach, Hydrol. Curr. Res., 2011 (2012) 118–125.

[27] X.-J. Hu, Y.-G. Liu, H. Wang, A.-W. Chen, G.-M. Zeng, S.-M. Liu, Y.-M. Guo, X. Hu, T.-T. Li, Y.-Q. Wang, Removal of Cu (II) ions from aqueous solution using sulfonated magnetic graphene oxide composite, Sep. Purif. Technol., 108 (2013) 189–195.

[28] M. Temkin, V. Pyzhev, Kinetics of ammonia synthesis on promoted iron catalysts, Acta Physiochim. URSS, 12 (1940) 217–222.

[29] A. Dąbrowski, Adsorption from theory to practice, Adv. Colloid Interface Sci., 93 (2001) 135–224.

[30] A.K. Meena, G. Mishra, P. Rai, C. Rajagopal, P. Nagar, Removal of heavy metal ions from aqueous solutions using carbon aerogel as an adsorbent, J. Hazard. Mater., 122 (2005) 161–170.
[31] Y. Hamzeh, A. Ashori, E. Azadeh, A. Abdulkhani, Removal of Acid Orange 7 and Remazol Black 5 reactive dyes from aqueous solutions using a novel biosorbent, Mater. Sci. Eng. C., 32 (2012) 1394–1400.
[32] S. Najafi, F. Salimi, C. Karami, Investigation of methylene blue adsorption in water solution using modified Fe_3O_4 magnetic nanoparticles by Guanidine, Pet. Sci., 28 (2018) 139–149.
[33] K. Parida, J. Das, Studies on ferric oxide hydroxides: II. Structural properties of goethite samples (α-FeOOH) prepared by homogeneous precipitation from $Fe(NO_3)_3$ solution in the presence of sulfate ions, J. Colloid Interface Sci., 178 (1996) 586–593.
[34] B. Stuart, B. George, P. Mclntyre, Modern Infrared Spectroscopy, John Wiley & Sons, New York, 1996.
[35] M. Ristić, E. De Grave, S. Musić, S. Popović, Z. Orehovec, Transformation of low crystalline ferrihydrite to α-Fe_2O_3 in the solid state, J. Mol. Struct., 834 (2007) 454–460.
[36] L. Zheng, X. Liu, Solution-phase synthesis of CuO hierarchical nanosheets at near-neutral pH and near-room temperature, Mater. Lett., 61 (2007) 2222–2226.
[37] A. Youssef, M. Al-Awadhi, M. Akl, Solid phase extraction and spectrophotometric determination of methylene blue in environmental samples using bentonite and acid activated bentonite from Egypt, J. Anal. Bioanal. Tech., 5 (2014) 1.
[38] B.S.K. Gorle, Adsorptive Crystallization of Organic Substances in Silica Aerogels from Supercritical Solutions, Friedrich-Alexander-Universität Erlangen-Nürnberg (FAU), 2009.
[39] M. Kosmulski, pH-dependent surface charging and points of zero charge II. Update, J. Colloid Interface Sci., 275 (2004) 214–224.
[40] A. Nezamzadeh-Ejhieh, M. Karimi-Shamsabadi, Comparison of photocatalytic efficiency of supported CuO onto micro and nano particles of zeolite X in photodecolorization of methylene blue and methyl orange aqueous mixture, Appl. Catal. A., 477 (2014) 83–92.
[41] M. Huang, C. Xu, Z. Wu, Y. Huang, J. Lin, J. Wu, Photocatalytic discolorization of methyl orange solution by Pt modified TiO_2 loaded on natural zeolite, Dyes Pigments, 77 (2008) 327–334.
[42] M. Ghaedi, A.G. Nasab, S. Khodadoust, M. Rajabi, S. Azizia, Application of activated carbon as adsorbents for efficient removal of methylene blue: kinetics and equilibrium study, J. Ind. Eng. Chem., 20 (2014) 2317–2324.
[43] S. Marković, A. Stanković, Z. Lopičić, S. Lazarević, M. Stojanović, D. Uskoković, Application of raw peach shell particles for removal of methylene blue, J. Environ. Chem. Eng., 3 (2015) 716–724.
[44] S. Cengiz, L. Cavas, Removal of methylene blue by invasive marine seaweed: *Caulerpa racemosa* var. *cylindracea*, Bioresour. Technol., 99 (2008) 2357–2363.
[45] B. Yan, Z. Chen, L. Cai, Z. Chen, J. Fu, Q. Xu, Fabrication of polyaniline hydrogel: synthesis, characterization and adsorption of methylene blue, Appl. Surf. Sci., 356 (2015) 39–47.
[46] S. Pal, S. Ghorai, C. Das, S. Samrat, A. Ghosh, A.B. Panda, Carboxymethyl tamarind-g-poly (acrylamide)/silica: a high performance hybrid nanocomposite for adsorption of methylene blue dye, Ind. Eng. Chem. Res., 51 (2012) 15546–15556.
[47] S.-L. Hii, S.-Y. Yong, C.-L. Wong, Removal of rhodamine B from aqueous solution by sorption on *Turbinaria conoides* (Phaeophyta), J. Appl. Phycol., 21 (2009) 625–631.
[48] N. Danesh, M. Hosseini, M. Ghorbani, A. Marjani, Fabrication, characterization and physical properties of a novel magnetite graphene oxide/Lauric acid nanoparticles modified by ethylenediaminetetraacetic acid and its applications as an adsorbent for the removal of Pb (II) ions, Synth. Met., 220 (2016) 508–523.
[49] M. Ciopec, C. Davidescu, A. Negrea, I. Grozav, L. Lupa, P. Negrea, A. Popa, Adsorption studies of Cr (III) ions from aqueous solutions by DEHPA impregnated onto Amberlite XAD7–Factorial design analysis, Chem. Eng. Res. Des., 90 (2012) 1660–1670.
[50] K.S. Sing, Reporting physisorption data for gas/solid systems with special reference to the determination of surface area and porosity (Recommendations 1984), Pure Appl. Chem., 57 (1985) 603–619.
[51] C. Lastoskie, K.E. Gubbins, N. Quirke, Pore size distribution analysis of microporous carbons: a density functional theory approach, J. Phys. Chem., 97 (1993) 4786–4796.
[52] A. Dąbrowski, P. Podkościelny, Z. Hubicki, M. Barczak, Adsorption of phenolic compounds by activated carbon—a critical review, Chemosphere, 58 (2005) 1049–1070.
[53] V.S. Mane, I.D. Mall, V.C. Srivastava, Kinetic and equilibrium isotherm studies for the adsorptive removal of Brilliant Green dye from aqueous solution by rice husk ash, J. Environ. Manage., 84 (2007) 390–400.
[54] P. Pimentel, M. Melo, D. Melo, A. Assuncao, D. Henrique, C. Silva, G. Gonzalez, Kinetics and thermodynamics of Cu (II) adsorption on oil shale wastes, Fuel Process. Technol., 89 (2008) 62–67.
[55] G. Sheng, J. Li, D. Shao, J. Hu, C. Chen, Y. Chen, X. Wang, Adsorption of copper (II) on multiwalled carbon nanotubes in the absence and presence of humic or fulvic acids, J. Hazard. Mater., 178 (2010) 333–340.
[56] G. McKay, Use of Adsorbents for the Removal of Pollutants from Wastewater, CRC Press, Boca Raton, FL, 1995.